

1 **Recent decrease in summer precipitation over the Iberian Peninsula**  
2 **closely links to reduction of local moisture recycling**

3 Yubo Liu<sup>1,2</sup>, Monica Garcia<sup>3,4</sup>, Chi Zhang<sup>1,5,6</sup>, Qihong Tang<sup>1,2\*</sup>

4

5 <sup>1</sup>Key Laboratory of Water Cycle and Related Land Surface Processes, Institute of Geographic  
6 Sciences and Natural Resources Research, Chinese Academy of Sciences, Beijing, China

7 <sup>2</sup>University of Chinese Academy of Sciences, Beijing, China

8 <sup>3</sup>[Research Center for the Management of Environmental and Agricultural Risks \(CEIGRAM\),](#)  
9 [E.T.S. de Ingeniería Agronómica, Alimentaria y de Biosistemas, Universidad Politécnica de](#)  
10 [Madrid, Avda. Senda del Rey, 13, 28040 Madrid, Spain](#)

11 <sup>4</sup>[Sino-Danish Center for Education and Research \(SDC\), 8000 Aarhus C, Denmark](#)

12 ~~Department of Environmental Engineering, Technical University of Denmark, Lyngby, 2800,~~  
13 ~~Denmark~~

14 <sup>5,6</sup>Key Laboratory of Land Surface Pattern and Simulation, Institute of Geographic Sciences and  
15 Natural Resources Research, Chinese Academy of Sciences, Beijing, China

16

17 **\*Correspondence:** Qihong Tang (tangqh@igsrr.ac.cn)

18

19 **Abstract**

20 The inherently dry summer climate of the Iberian Peninsula (IP) is undergoing drought  
21 exacerbated by more intense warming and reduced precipitation. Although many  
22 studies have studied changes in summer climate factors, it is still unclear how the  
23 changes in moisture contribution from the sources lead to the decrease in summer  
24 precipitation. This study investigates the differences in the IP precipitation shed between  
25 1980-1997 and 1998-2019 using the Water Accounting Model-2layers with ERA5 data,  
26 and assesses the role of local [moisture](#) recycling and external moisture in reducing  
27 summer precipitation. Our findings indicate that the moisture contributions from the  
28 local IP, and from the west and the east of the precipitation shed contributed 1.7, 3.6 and  
29 1.1 mm mon<sup>-1</sup> less precipitation after 1997 than before 1997, accounting for 26 %, 57 %  
30 and 17 % of the main source supply reduction, respectively. The significant downward  
31 trend of the IP local [moisture](#) recycling closely links to the disappearance of the wet  
32 years after 1997 as well as the decrease of local contribution in the dry years. Moreover,  
33 the feedback between the weakened local moisture recycling and the drier land surface  
34 can exacerbate the local moisture scarcity and summer drought.

35

## 36 1. Introduction

37 The Iberian Peninsula (IP) is located in the Mediterranean ~~area~~[basin](#), which is  
38 among the global “hotspots” of climate change. The IP precipitation is characterized by  
39 the diverse climatic regimes and high spatial variability as a consequence of its  
40 geographic position between the Atlantic Ocean and the Mediterranean Sea and its  
41 orographic configuration. In responding to climate change with frequent heatwaves and  
42 above-average warming, the IP is experiencing widespread decreases in precipitation,  
43 especially in summer (Brogli et al., 2019; Cramer et al., 2018; Rajczak and Schär, 2017).  
44 This reduction in summer precipitation is a major driver of water resource depletion  
45 and the evolution of drought (Lopez-Bustins and Lemus-Canovas, 2020; Páscoa et al.,  
46 2021; Teuling et al., 2013). To clarify the reason for the decrease in summer  
47 precipitation, it is necessary to explain the changes in moisture contribution from the  
48 [sources](#), such as local [moisture](#) recycling and external sources.

49 Analysis of source supply and transportation in the hydrological cycle has become  
50 one efficient way to understand well regional precipitation. With the introduction of the  
51 concept of precipitationshed (Keys et al., 2014; Keys P. W. et al., 2011), which better  
52 reveals the contribution from upwind evaporation sources to [the](#) precipitation in  
53 downwind sink region, it is more scientific and systematic to explain the precipitation  
54 variations by using the fluctuations of moisture contribution as a precursor. Given the  
55 importance of studying the source of precipitation, that is, precipitationshed, a variety  
56 of methods have been developed and adopted, including physical isotope analysis

57 (Bonne et al., 2014), and numerical analytical models, either online methods running  
58 in parallel with climate models (Damián and Gonzalo, 2018; Stohl and James, 2004,  
59 2005), or offline “posteriori models” (van der Ent and Savenije, 2011; van der Ent et  
60 al., 2010; van der Ent et al., 2013). [Furthermore, the local moisture recycling, which](#)  
61 [describes the local precipitation-evaporation feedback relationship, has been proposed](#)  
62 [to further differentiate regional local and external contributions to the designated area.](#)  
63 Although the mechanisms of these studies are different, they all emphasize that the  
64 constantly changing source-sink relationship of atmospheric moisture is an essential  
65 part of climate change research as global change continues.

66 Gimeno et al. (2010) comprehensively investigated the atmospheric moisture  
67 sources of the IP precipitation at different scales, and identified the tropical–subtropical  
68 North Atlantic corridor, the surrounding Mediterranean Sea and the local IP as ~~the~~  
69 important moisture regions. The high precipitation in the cold season is mainly  
70 dominated by westerly wind regimes. The mid-latitude atmospheric dynamics, such as  
71 the baroclinic synoptic-scale perturbations from the Atlantic and the polar jet stream,  
72 as well as the high moisture supply from an Atlantic “tropospheric river” seem to be  
73 responsible for the abundant precipitation during the cold season (Cortesi et al., 2013;  
74 Ulbrich et al., 2015; Zhu and Newell, 1998). Compared to the rainy winter, the summer  
75 with very low precipitation receives less attention. The subtropical location under the  
76 descending air extending from the North Atlantic subtropical high controls low summer  
77 precipitation over the IP, and local convective events increase the importance of local

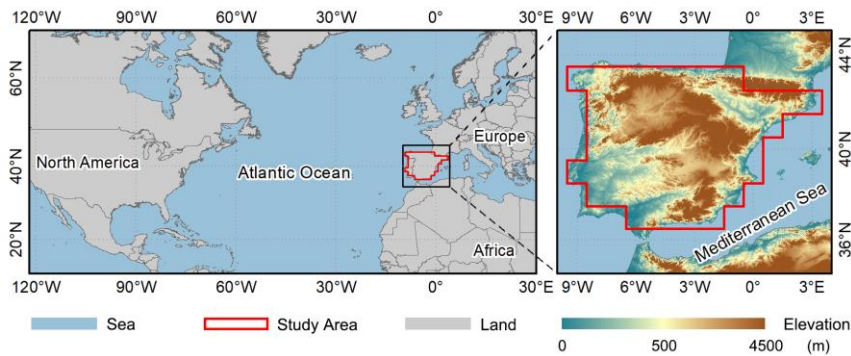
78 [moisture](#) recycling during summer (Serrano et al., 1999). Accordingly, the summer IP  
79 precipitation, [with](#) a significant proportion of ~~which is taken up by~~ the locally recycled  
80 ~~water vapor~~[moisture](#), is completely different from the [winter IP](#) precipitation ~~in winter~~  
81 that is dominated by the ~~moisture transported over long distances from distant~~ external  
82 ~~sources~~[moisture](#).

83 In recent decades, the increasing severity of summer drought in the IP, which is  
84 closely related to precipitation variations, has attracted more attention. Several  
85 mechanisms, including soil-atmosphere interactions (Boé and Terray, 2014), cloud  
86 processes (Lenderink et al., 2007; Tang et al., 2012) and large-scale circulation changes  
87 (Boé et al., 2009; Brogli et al., 2019; Kröner et al., 2017), have been found to be  
88 potentially important for this complex summer climate change, which also appear to  
89 have an impact on [the](#) precipitation reduction. [Such anomaly of summer precipitation](#)  
90 [in the sink is inevitably linked to source changes, but](#) ~~However~~, there is still a lack of  
91 [knowledge about how source moisture contributes to](#) ~~such summer~~ precipitation decline,  
92 ~~in terms of changes in the moisture contribution from the source~~. Therefore, tracing the  
93 precipitation shed of the IP and quantifying the moisture contributions can provide us  
94 with a new perspective to analyze the changes in IP precipitation. This study aims to  
95 evaluate the moisture contribution of [the](#) local [moisture](#) recycling and external sources  
96 to the ~~reduction of IP~~ summer precipitation [over the IP. It can provide a scientific](#)  
97 [reference for the prediction and management of droughts that may be caused by](#)  
98 [precipitation reduction from the perspective of source moisture contribution.](#)

99 **2. Study Area, Data and Methods**

100 2.1 Study area

101 The IP is located in southwestern Europe at midlatitudes of the northern  
102 hemisphere. It covers Portugal and the mainland of Spain. The geographic location of  
103 IP is shown in Fig. 1(a) (36°N-44°N, 10°W-3°E) in a transition zone between  
104 midlatitude and subtropical atmospheric circulation regimes. It has a complex  
105 topography, surrounded by the Atlantic Ocean and Mediterranean Sea, and **high**  
106 **elevated** in the middle and northeast. The topographic and coastal processes affect water  
107 vapor transport, forming a spatial precipitation gradient from **the** northwest to **the**  
108 southeast. Extracted from the land-sea mask provided by European Centre for Medium-  
109 range Weather Forecasts (ECMWF), the red outline area composed of multiple single  
110 1×1 degree grids is our study area of **the** IP.



112 **Figure 1** Map of the IP (the area within the closure of the red line) on a grid of 1°×1° as the target  
113 region.

114

## 115 2.2Data

116 The newest reanalysis data held in ECMWF data archive, [the ERA5 dataset](#)  
117 downloaded from the Copernicus Climate Change Service (C3S) Climate Data Store  
118 (CDS) is used in this study (Hersbach et al., 2020). The variables include surface  
119 pressure, precipitation, evaporation, total column water, and vertical integrated  
120 eastward and northward atmospheric water fluxes (including cloud liquid water flux,  
121 cloud frozen water flux and water vapor flux) on single level, as well as the horizontal  
122 U/V components of wind fields and specific humidity at the lowest 23<sup>rd</sup> pressure levels  
123 (200-1000hPa). The time resolution and spatial resolution selected for these data are 1  
124 hour and 1×1 degree, respectively. This dataset covers the period from 1980 to 2019.  
125 Compared to the old version reanalysis data (e.g., ERA-Interim or ERA-40), ERA5  
126 combines vast amounts of historical observations into global estimates using more  
127 advanced modelling and data assimilation systems (Hersbach et al., 2020).

128 ~~To avoid the uncertainty of ERA5 precipitation as~~ [the ERA5 precipitation is a](#)  
129 global forecast dataset [with some uncertainties](#), its reliability in the IP [region](#) needs to  
130 be verified. Therefore, an observational gridded dataset generated from a dense network  
131 of stations over the IP, named [the Iberia01](#) (Herrera et al., 2019), is used to verify the  
132 accuracy of [the ERA5 precipitation data](#). [The Iberia01](#) provides the daily precipitation  
133 for the period of 1971-2015 at 0.1×0.1 degree.

## 134 2.3 Model and methods

### 135 2.3.1 Water Accounting Model-2layers

136 Water Accounting Model-2layers (WAM-2layers) is an offline Eulerian method  
137 tracking the moisture cycle forwards or backwards that quantifies the source-sink  
138 relations (van der Ent et al., 2013; van der Ent et al., 2014). Its backward algorithm was  
139 used in this study to trace the precipitationshed of the IP. The model of WAM-2layers  
140 is an updated version of the original WAM. The water vapor balance equation in the  
141 WAM-2layers algorithm maintains the premise that the atmosphere is well mixed, but  
142 compared with the previous model, it takes the stratification of the atmosphere into  
143 consideration. Thus, when the algorithm is applied to a specific region, the calculation  
144 is as follows,

$$145 \quad \frac{\partial W_{l,r}}{\partial t} + \frac{\partial(W_{l,r}u)}{\partial x} + \frac{\partial(W_{l,r}v)}{\partial y} = E_{l,r} - P_{l,r} \pm F_{v,r} + \alpha_{l,r} \quad (1)$$

146 where  $W$  is the atmospheric moisture storage, or namely, precipitable water;  $t$  is time;  $u$   
147 and  $v$  are the wind components in  $x$  (zonal) and  $y$  (meridional) direction, respectively;  
148  $E$  is evaporation;  $P$  is precipitation;  $F_v$  is the vertical moisture transport between the  
149 bottom and top layer;  $\alpha$  is a residual term, [which is resulted from the ERA5 data](#)  
150 [assimilation and the coarser resolution scheme in the model calculation \(van der Ent et](#)  
151 [al., 2014\)](#); the subscript  $l$  represents the portion in layer  $l$  (either the bottom layer or the  
152 top layer), and the subscript  $r$  represents the tagged portion provided by the source  
153 region.

154 Based on the assumption of a well-mixed atmosphere (Burde, 2010; Goessling and  
 155 Reick, 2013), the moisture contribution, that is, the tagged evaporation  $E_r$ , can be  
 156 calculated considering that the ratio of tagged to total atmospheric water storage is equal  
 157 to the ratio of tagged to total evaporation, as shown in Eq. (2). Considering the proposed  
 158 retention time of atmospheric moisture is about 1 week to 10 days (Numaguti, 1999),  
 159 we set the backtracking time as 1 month longer for summer precipitation to make sure  
 160 that more than 90 % of the precipitation can be redistributed to the surface (Zhang et  
 161 al., 2017).

$$162 \quad E_r(t, x, y) = E(t, x, y) \frac{W_r(t, x, y)}{W(t, x, y)} \times E(t, x, y) \quad (2)$$

163 The main moisture source suppling IP summer precipitation, ~~that is, is defined as~~  
 164 the 90<sup>th</sup> percentile precipitationshed in this study. ~~It is further~~ divided into subregions  
 165 to evaluate the role of the contribution from each area, such as the local moisture  
 166 recycling, which demonstrates the contribution of local evaporation to the IP  
 167 precipitation, and the external advection moisture, which describes the non-local  
 168 evaporation contribution to the IP precipitation. The contribution ratio (CR) of a  
 169 subregion ~~For each of the partitioned source region (A) is defined as,~~ the proportion of  
 170 the moisture contribution from ~~all grids covered by~~ it to the total contribution from the  
 171 main source region ( $MS$ ) ~~is the contribution ratio (CR),~~ which is calculated as the  
 172 following Eq. (3). The precipitation recycling ratio of the IP can be substituted with the  
 173 IP local contribution ratio  $CR_{IP}$ .

174 
$$CR_A = \frac{\sum E_r(t, x, y|A)}{\sum E_r(t, x, y|MS)} \times 100\% \quad (3)$$

175 2.3.2 Significance test

176 The slope significance of trend fitting and the significance of the difference in the  
 177 means are tested using Student t-test in this study. Additionally, the [sliding t-test, as a](#)  
 178 [method of](#) mutation analysis, [is used to detect whether and when the sample mean in](#)  
 179 ~~[the for detecting significant mutation in IP](#)~~ precipitation series [changed significantly](#)  
 180 ~~[is the sliding t-test,](#)~~

181 
$$T = \frac{\frac{1}{n_1} \sum_{t=1}^{n_1} x - \frac{1}{n_2} \sum_{t=n_1+1}^{n_1+n_2} x}{\frac{(n_1-1)S_1^2 + (n_2-1)S_2^2}{n_1+n_2-2} \sqrt{\frac{1}{n_1} + \frac{1}{n_2}}} \quad (4)$$

182 where  $x$  is the precipitation series to be tested,  $n_1$  and  $n_2$  are step lengths set for two  
 183 sequences before and after the moving point, and  $S_1^2$  and  $S_2^2$  are the variances of the two  
 184 sequences which can be calculated as following.

185 
$$S_1^2 = \frac{1}{n_1-1} \sum_{t=1}^{n_1} (x - \frac{1}{n_1} \sum_{t=1}^{n_1} x)^2 \quad (5)$$

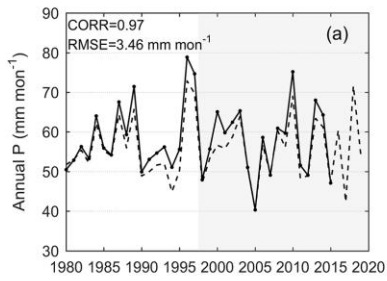
186 
$$S_2^2 = \frac{1}{n_2-1} \sum_{t=n_1+1}^{n_1+n_2} (x - \frac{1}{n_2} \sum_{t=n_1+1}^{n_1+n_2} x)^2 \quad (6)$$

187 **3. Results**

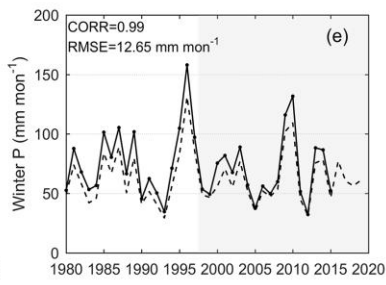
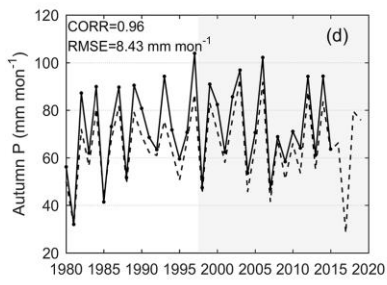
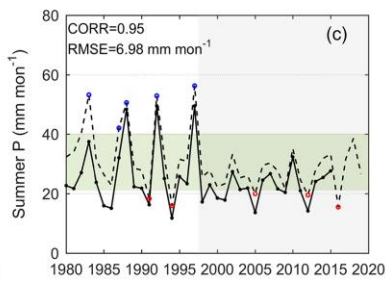
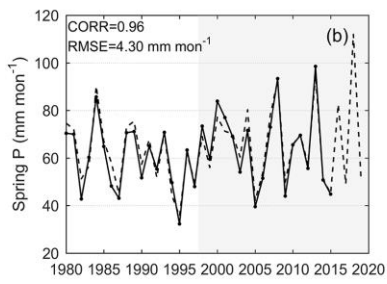
188 3.1 Evaluation and variation of precipitation data

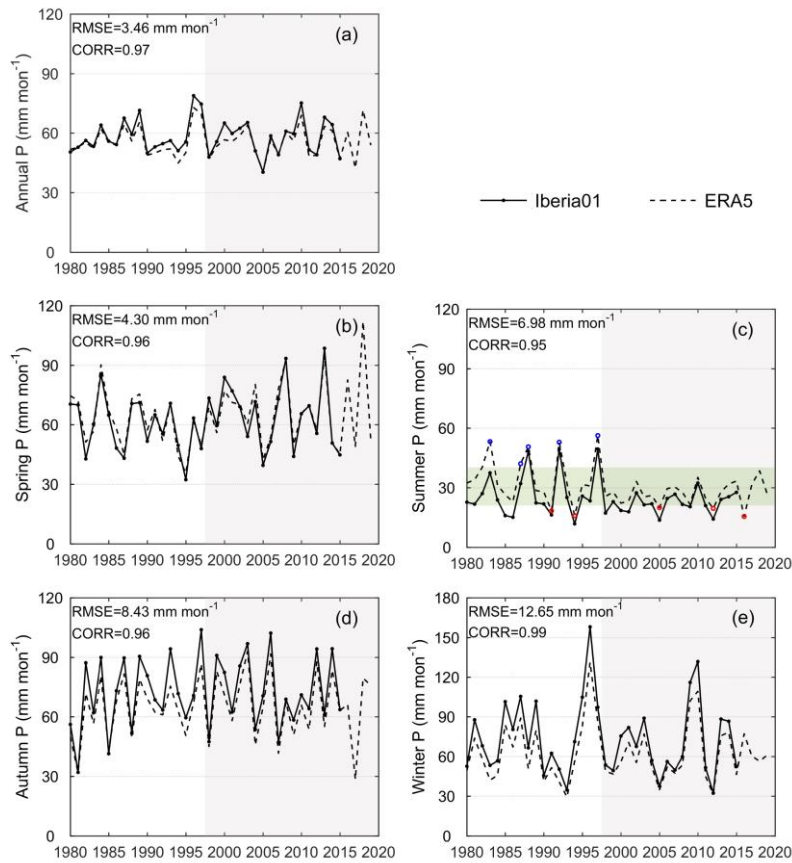
189 The precipitation time series of [the](#) ERA5 and [the](#) Iberia01 data are shown in Fig.  
 190 2. The fluctuations and variations of [the](#) ERA5 precipitation data are in good agreement  
 191 with the observed data on both annual and seasonal scales, together with all correlation  
 192 coefficients higher than 0.95. The average annual precipitation over the IP is about

193 55.66 mm mon<sup>-1</sup> from ERA5 and 58.07 mm mon<sup>-1</sup> from Iberia01, respectively.  
194 Compared with the observed data, the reanalysis data slightly underestimates the IP  
195 precipitation with the root mean square error (RMSE) of 3.46 mm mon<sup>-1</sup> on the annual  
196 scale. The comparison of seasonal precipitation shows that [the](#) ERA5 is lower than the  
197 observed Iberia01 value in the rainy seasons (both winter and autumn), but higher in  
198 the dry summer. The RMSE between the two datasets of seasonal precipitation is in the  
199 range of 4.30-12.65 mm mon<sup>-1</sup>. Since [the](#) Iberia01 data is the grid data interpolated from  
200 observation site data (Herrera et al., 2019), some of the deviations between the ERA5  
201 and [the](#) Iberia01 precipitation can be partially affected by the interpolation process  
202 rather than solely the result of the error generated by the reanalysis process. In general,  
203 [the](#) ERA5 precipitation data shows the characteristics of IP precipitation reasonably  
204 well and thus is suitable for studying the changes.



— Iberia01    - - - ERA5

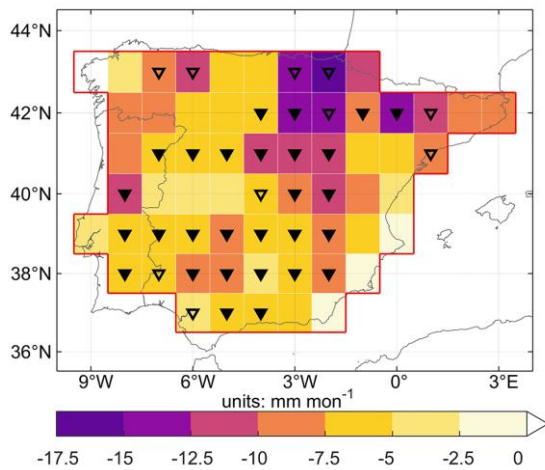


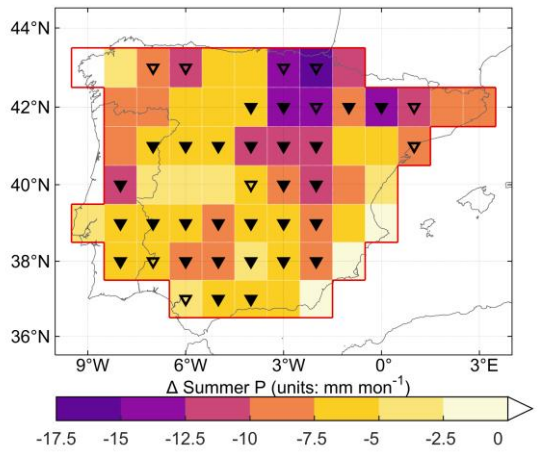


206  
 207 **Figure 2** Variations of IP (a) annual precipitation (a), (b) spring (March, April and May, b), (c)  
 208 summer (June, July and August, c), (d) autumn (September, October and November, d) and (e)  
 209 winter (December, January and February, e) during 1980-2019. [The white shading is for the period](#)  
 210 [1980-1997 and the grey shading is for the period 1998-2019.](#) The green shading covers the interval  
 211 of one standard deviation of summer precipitation. The years with summer ERA5 precipitation  
 212 exceeding the range of the green shading interval are circled in blue and red.

213 Only in summer, the mutation analysis [results](#) of the two sets of precipitation data,

214 [the Iberia01 \(T value: 1.83\)](#) and [the ERA5 \(T value: 1.86\)](#), both show statistically  
215 significant changes [at 0.1 level in the year 1997](#). Accordingly, the entire 40-year period  
216 is divided into two periods, 1980-1997 and 1998-2019, to compare the difference in  
217 summer precipitation between the two periods. The average summer precipitation is  
218 34.89 and 27.17 mm mon<sup>-1</sup> before and after 1997, respectively. Compared with 1980-  
219 1997, the average summer precipitation during 1998-2019 decreases by 7.72 mm  
220 (22.13 %) in the whole study area. On the grid scale, almost all grids have less  
221 precipitation after 1997, and more than half of all grids show the statistically significant  
222 reductions (Fig. 3). However, this change is unevenly distributed in space, as shown by  
223 the greater reduction in the grids on the northeastern IP that can even exceed 10 mm  
224 mon<sup>-1</sup>.





226

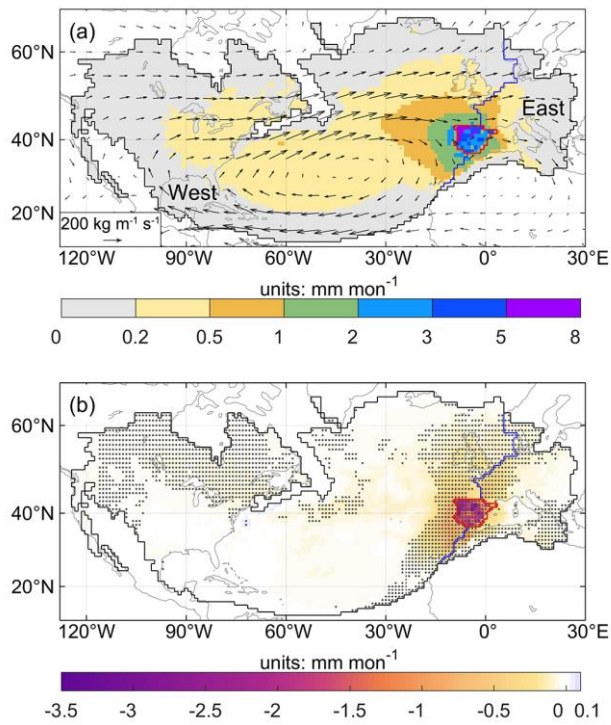
227 **Figure 3** The difference of average summer precipitation over the IP between 1998-2019 and 1980-  
 228 1997 (average of 1998-2019 minus average of 1980-1997). The triangles indicate [that](#) the  
 229 differences are significant at 0.05 (solid) and 0.1 (hollow) level.

230 For summer precipitation, the dry years (1991, 1994, 2005, 2012 and 2016) and  
 231 the wet years (1983 1987 1988 1992 and 1997) are selected, which are circled in Fig.  
 232 2(c). A wet year is defined as the year in which the precipitation is more than one  
 233 standard deviation above the average precipitation, and similarly, the precipitation in a  
 234 dry year is lower than a standard deviation range. Accordingly, the division of time  
 235 period also applies to the precipitation series of the dry and wet years. It is specifically  
 236 observed that the dry years are ~~separated~~ [distributed in both two periods](#), with the  
 237 average precipitation of 17.15 and 18.34 mm mon<sup>-1</sup> before and after 1997, whereas [the](#)  
 238 wet years occur before 1997 with an average of 51.03 mm mon<sup>-1</sup> but disappear after  
 239 1997.

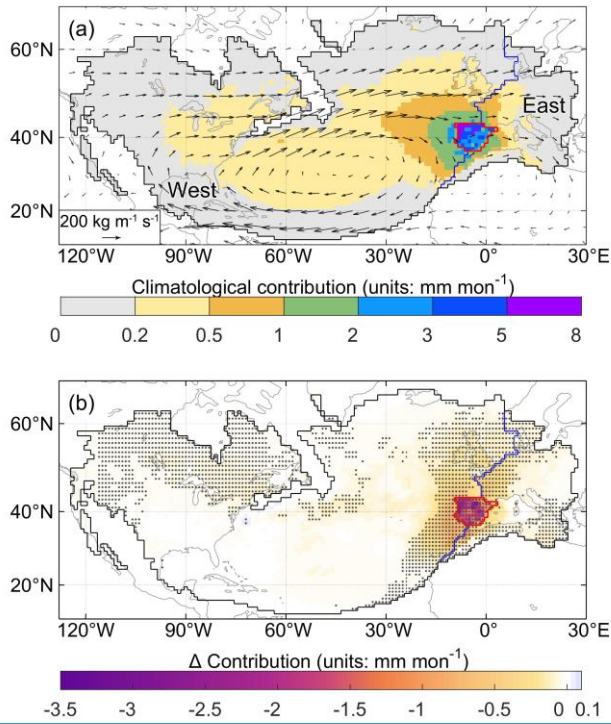
### 240 3.2 Changes in summer precipitation shed and regional contributions

241 From 1980 to 2019, [the average value of the IP summer precipitation is about](#)  
242 [30.64 mm mon<sup>-1</sup>](#). ~~An average of 28.53 mm mon<sup>-1</sup>~~. [More than 93 % of this summer](#)  
243 precipitation has been tracked by the global surface [through modelling, averaging 28.53](#)  
244 [mm mon<sup>-1</sup>](#). ~~exceeding 93 % of IP summer precipitation with an average of 30.64 mm~~  
245 ~~mon<sup>-1</sup>~~. The climatology of the moisture contribution during the 40 years is shown in  
246 Fig. 4 (a). The moisture contribution to [the](#) IP generally decreases as its distance to IP  
247 increases. Although the precipitation shed of [the](#) IP summer precipitation is global in  
248 scope, the contribution of the area far away is negligible to be considered. Therefore,  
249 the 90<sup>th</sup> precipitation shed enclosed by the black line in Fig. 4 is given full attention as  
250 the main moisture source region in the following text. The main moisture source of the  
251 IP covers not only the local grids in the study region, but also several of non-local land  
252 and oceanic areas. Due to the dominance of the westerlies in [the](#) tropical–subtropical  
253 North Atlantic corridor (Gimeno et al., 2010), ~~as shown by the circulation in the Fig.~~  
254 ~~4(a)~~, most of the non-local source grids are located in the North American land and [the](#)  
255 North Atlantic Ocean ~~to the~~ west of the study area, [which jointly form a relatively](#)  
256 [stable atmospheric basin in the global atmospheric moisture networks \(Zhang et al.,](#)  
257 [2020\) under the influence of the summer anticyclonic structure \(Fig. 4\(a\)\).](#) The other  
258 source grids are located east of [the](#) North Atlantic Ocean and the IP, which is the  
259 downwind zone for water vapor transport, covering Western Europe and the

260 Mediterranean. [These eastern regions with positive atmospheric moisture divergence](#)  
261 [provide a net water flux to the atmosphere, moisten the air parcels flowing towards the](#)  
262 [surrounding land, and become the main short-term moisture sources affecting the IP,](#)  
263 [especially the eastern IP \(Gimeno et al., 2010; Vázquez et al., 2020\).](#) Hence, the main  
264 moisture sources are divided into the three partial regions of the local IP, the west and  
265 the east by the boundary of the study area and the eastern boundary of the Atlantic  
266 Ocean (red and blue lines in Fig. 4), and the contribution of each region to [the](#) IP  
267 precipitation can be quantified and compared.



268



269

270 **Figure 4** (a) Climatological 90<sup>th</sup> precipitation shed of the IP sink region and moisture contribution

271 to the IP summer precipitation from 1980 to 2019. The black outlines show the 90<sup>th</sup> precipitation shed

272 boundary during the 40 years. The vectors represent the climatological monthly water vapor flux.

273 The red line encloses the study area, and the blue line divides the precipitation shed excluding the IP

274 into the west (left area) and the east (right area) regions. (b) Differences in the moisture contribution

275 in the 90<sup>th</sup> precipitation shed between 1998-2019 and 1980-1997 (average of

276 1998-2019 minus average of 1980-1997). The dots indicate 0.1 significance of the difference.

277 Affected by the transport distance, the grids with high contribution are located in

278 and around the target IP region, with the maximum values for grids in the northwest

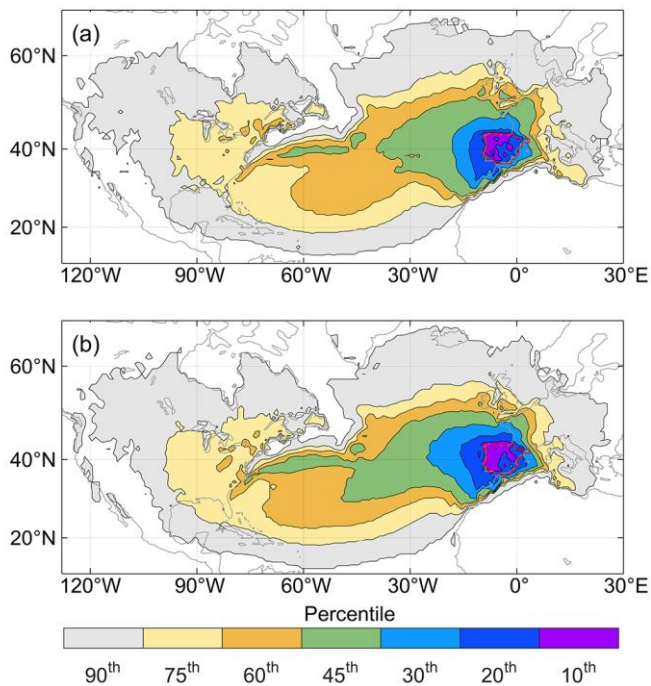
279 corner of the IP. The local IP contributes 3.46 mm mon<sup>-1</sup> average summer precipitation,

280 with the precipitation recycling ratio of around 13.26 % during the 40 years. The west,  
281 as the largest sub-region of the precipitationshed, contributes the most summer  
282 precipitation of 19.38 mm mon<sup>-1</sup> and occupies 76.06 % of the tracked precipitation  
283 averagely. While the east region, which is in an unfavorable downwind position in the  
284 summer circulation, provides only 2.81 mm mon<sup>-1</sup> summer precipitation, accounting  
285 for 10.68 %.

286 The difference in moisture contribution obtained from the 1998-2019 period minus  
287 the 1980-1997 period is shown in Fig. 4(b). Almost all grid contributions show a  
288 decrease after 1997. The grids with a large moisture contribution decline are mainly  
289 concentrated in the IP, with the maximum reduction exceeding an average of 3 mm  
290 mon<sup>-1</sup> ([more than 50% of its climatological moisture contribution](#)). Compared with  
291 other non-local source grids, the grids with higher contributions along the east coast of  
292 the North Atlantic near the IP also have a slight but significant reduction in contribution.

293 Due to the uneven distribution of grid contribution reduction in space, the area of  
294 different percentile precipitationsheds differs in the two periods. The areas with  
295 different colors in the distribution map of Fig. 5 represent the precipitationshed  
296 boundaries at different percentiles in the two periods. During 1998-2019, the  
297 precipitationshed boundary of each percentile extends westward in varying degrees  
298 compared with those before 1997. The top decile of the contribution is still in the  
299 western half of the IP. In the North Atlantic, the westward expansion of the western  
300 boundary of the precipitationsheds is conspicuous, especially the 45th and 60th

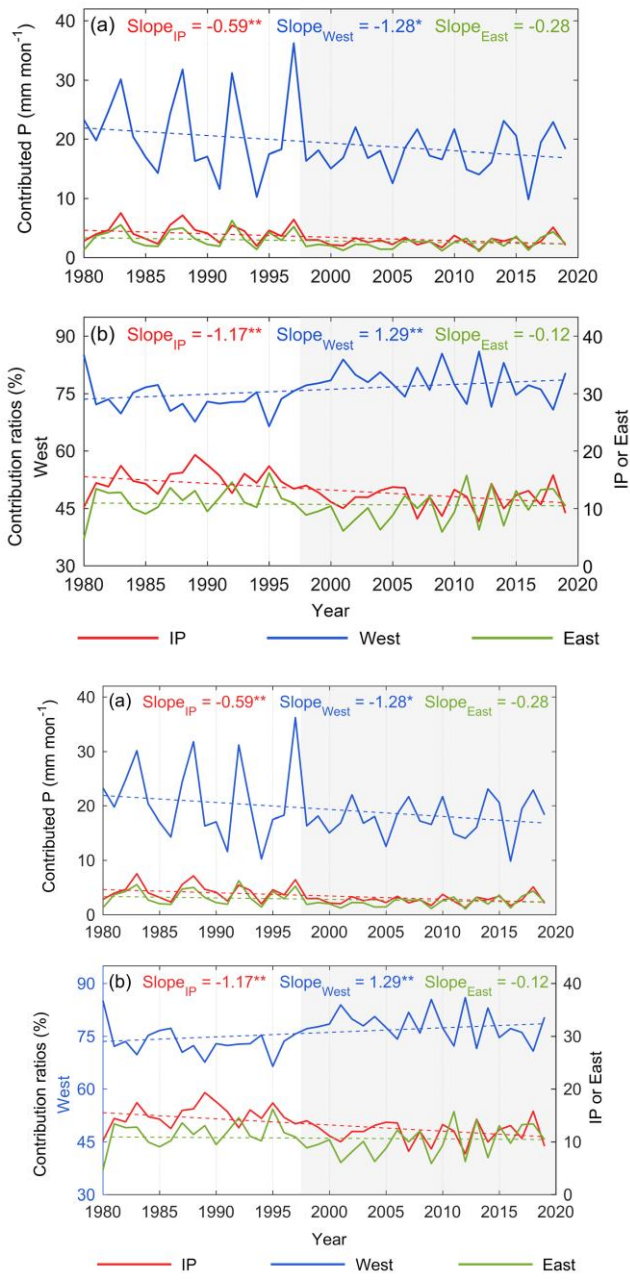
301 percentile precipitationsheds shown in orange and green color in Fig. 5(a, b). This  
 302 westward extension implies that the significant and substantial reduction in the  
 303 contribution of the local grids and its surrounding grids results in a decrease in the  
 304 proportion of these areas. Therefore, for the same percentile of the precipitationshed,  
 305 only a smaller area concentrated by high-contribution grids is sufficient before 1997.  
 306 However, a larger area is required for the same proportion after 1997.



307  
 308 **Figure 5** Different percentile precipitationsheds during the two periods (a) 1980-1997 (a) and (b)  
 309 1998-2019 (b). The proportion of the cumulative contribution to the IP precipitation from all areas  
 310 enclosed by the contour line is the percentile indicated by the corresponding color.

311 Figure 6(a) shows the quantified precipitation contributed by the local IP, the west  
 20

312 and the east regions. The negative slopes in Fig. 6(a) indicate that the summer  
313 precipitation contributed by these three regions has a downward trend, especially  
314 significant for the IP and the west with slopes of  $-0.59$  and  $-1.28 \text{ mm mon}^{-1} \text{ decade}^{-1}$ .  
315 These decreasing trends cause a  $6.38 \text{ mm mon}^{-1}$  difference in precipitation from the  
316 main source region in the two periods, which explains 82.64 % of the total reduction in  
317 the IP summer precipitation ( $7.72 \text{ mm mon}^{-1}$ ). In terms of the difference in the average  
318 values of each region, the precipitation contributed by the local IP, the west and the east  
319 significantly decreases from  $4.38$ ,  $21.37$  and  $3.41 \text{ mm mon}^{-1}$  in 1980-1997 to  $2.71$ ,  
320  $17.76$  and  $2.32 \text{ mm mon}^{-1}$  in 1998-2019, respectively. 26.32 %, 56.53 % and 17.15 %  
321 of the difference in the main source supply between the two periods are due to the  
322 contribution decline from the local IP, the west and the east, respectively.



323

324

325 **Figure 6** Variations of (a) contributed precipitation (a-unit of the slope: mm mon<sup>-1</sup> decade<sup>-1</sup>) and (b)

326 contribution ratios (unit of the slope: % decade<sup>-1</sup>) from the IP, the west and the east region during  
327 1980-2019 summer. \*\*\* and \*\* represent 0.05 and 0.1 level significance of the trend.

328 The variation and trend of the contribution ratio of each region are shown in Fig.  
329 6(b). The proportion of contributions from the local IP and the east shows a decreasing  
330 trend throughout the 40 years with the slope of -1.17 % decade<sup>-1</sup> and -0.12 % decade<sup>-1</sup>,  
331 which is consistent with the decreasing trends of their absolute contributions.  
332 Conversely, although the precipitation contributed by the west shows a decreasing trend,  
333 its proportion is significantly increasing and the slope is 1.29 % decade<sup>-1</sup>. The average  
334 contribution ratios of the local IP and the east decrease from 15.05 % and 11.49 %  
335 before 1997 to 11.79 % and 10.02 % after 1997, while the ratio of the west increases  
336 from 73.46 % to 78.19 %.

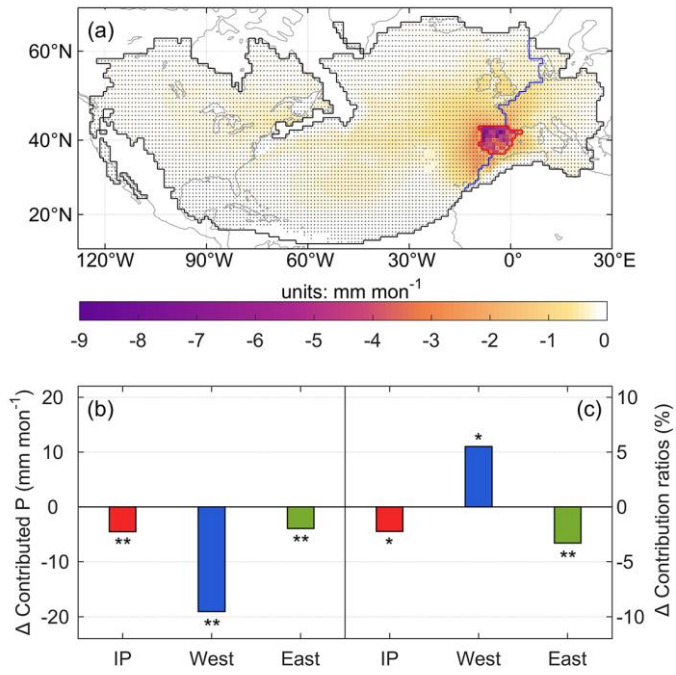
### 337 3.3 Differences in wet years and dry years

338 The dry years (1991, 1994, 2005, 2012 and 2016) and the wet years (1983 1987  
339 1988 1992 and 1997) are selected as described in section 3.1. Of the two divided periods,  
340 all the wet years only occur before 1997, while the dry years are distributed in both  
341 periods with no decrease in its average value. This represents that although the average  
342 summer precipitation after 1997 is reduced significantly compared with the previous  
343 period, there is no decrease in the valley value of the precipitation series. Thus, the  
344 disappearance of the wet years during 1998-2019 caused by the decrease of the  
345 precipitation series peaks directly reflects the recent decrease in [the](#) IP summer

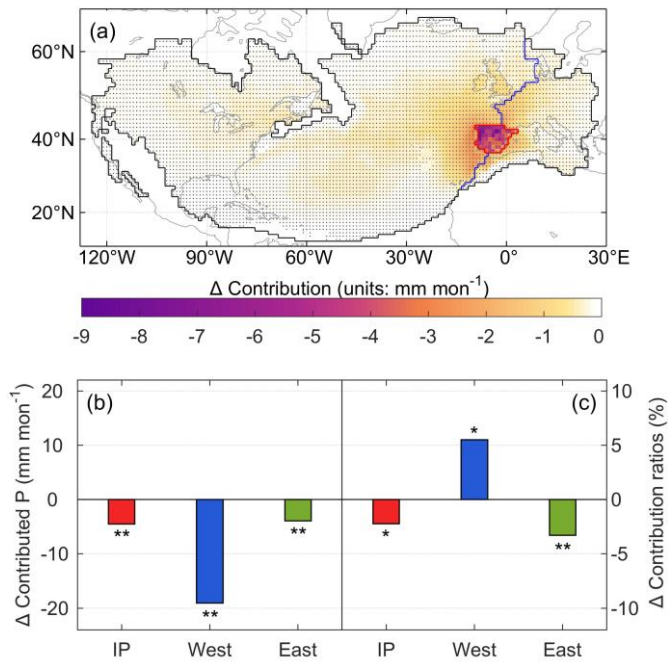
346 precipitation.

347       During the entire 40 years, ~~the differences~~ in moisture contribution within the 90<sup>th</sup>  
348 precipitation shed of the IP summer precipitation between the wet and dry years ~~is-are~~  
349 shown in Fig. 7(a). In the dry years, the significant reduction in the moisture  
350 contribution from all grids in the main source region induces much lower precipitation  
351 than in the wet years. On the grid scale, the larger declines primarily happened in the  
352 local IP, and the grids with the largest drop, close to 9 mm mon<sup>-1</sup>, are mainly  
353 concentrated in the west and the north of the IP. In each source region, an average of  
354 6.41, 30.74 and 5.34 mm mon<sup>-1</sup> of the summer IP precipitation is provided from the  
355 local IP, the west and the east in the wet years, with 15.15 % recycling ratio, 72.19 %  
356 and 12.66 % contribution ratio. While in the dry years, the average precipitation  
357 contributed from each region is 1.92, 11.66 and 1.40 mm mon<sup>-1</sup>, accounting for 12.93 %,  
358 77.70 % and 9.37 %, respectively. All three regions contribute more to summer  
359 precipitation in the wet years than in the dry years, and compared with the dry years,  
360 the contribution ratios of the local IP and the east in the wet years are also higher. The  
361 disappearance of the wet years ~~during 1998-2019~~ after 1997, ~~further motivates similar~~  
362 ~~changes between the two periods~~ compared with those before 1997, exacerbates the  
363 decline in contributions from all three sources, due to the high moisture supply in the  
364 wet years. The decrease in the frequency of the wet years with higher local moisture  
365 recycling ratio and higher contribution ratio of the east leads to an increase in the  
366 proportion of the summer precipitation originating from the remaining other region,

367 namely the west, during the same period.



368

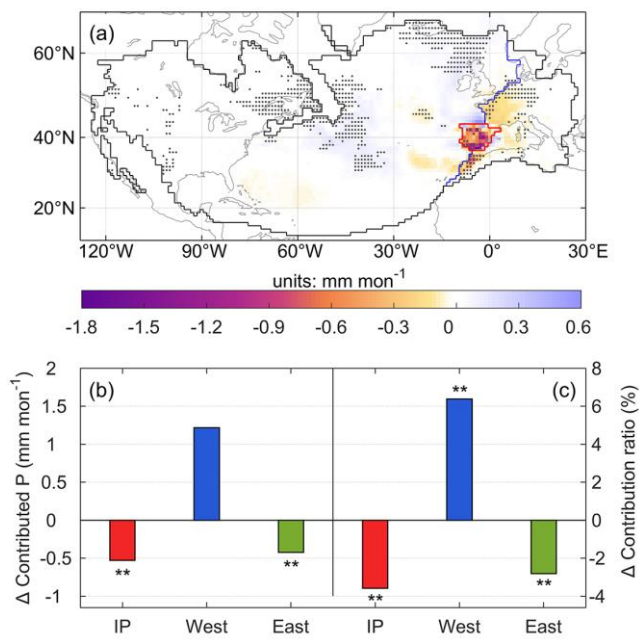


369

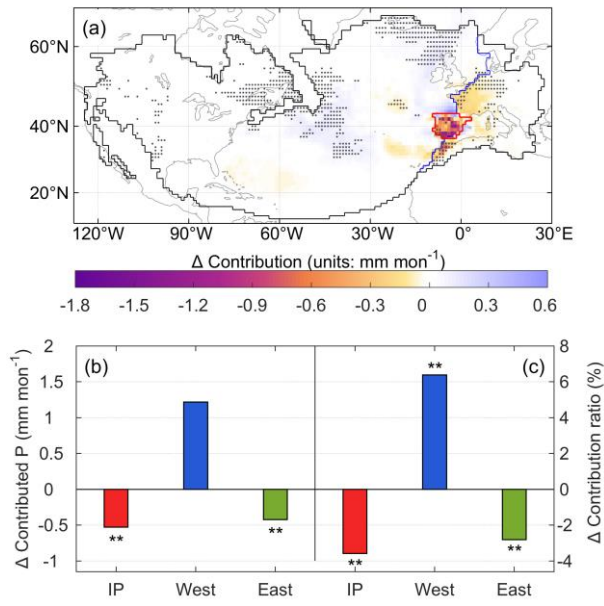
370 **Figure 7** (a) Differences in the moisture contribution in the 90<sup>th</sup> precipitation shed between the dry  
 371 years and the wet years (average of the dry years minus average of the wet years). The dots indicate  
 372 0.1 significance of the difference. The changes in (b) average precipitation contributed from each  
 373 region (b) and (c) their average contribution ratios (c) between the dry years and the wet years. ‘\*\*\*’  
 374 and ‘\*’ represent 0.05 and 0.1 level significance of the difference.

375 The dry years in the two periods have been divided and compared with each other,  
 376 and the differences between the two periods are shown in Fig. 8. From the distribution  
 377 of differences, the grids with reduced moisture contribution are mainly located in the  
 378 IP and the east region, and the southern part of the IP has the largest decrease (Fig. 8(a)).  
 379 Mainly dominated by these negatively changing grids, both the absolute contribution

380 and the contribution ratio of the local IP and the east have dropped significantly, with  
 381 0.53 and 0.42 mm mon<sup>-1</sup> decrease in contributed precipitation and 3.58 % and 2.81 %  
 382 contribution ratio reduction, respectively (Fig. 8(b, c)). For the west region, however,  
 383 it raises the moisture contribution to the summer precipitation by 1.22 mm mon<sup>-1</sup> in the  
 384 dry years after 1997, causing a 6.39 % increase in its contribution ratio. Despite the dry  
 385 years with no decrease precipitation between the two periods, the decrease in the local  
 386 moisture recycling is still noticeable.



387



388

389 **Figure 8** (a) Differences in the moisture contribution in the 90<sup>th</sup> precipitation shed in the dry years  
 390 between 1998-2019 and 1980-1997 (average of 1998-2019 minus average of 1980-1997). The dots  
 391 indicate 0.1 significance of the difference. The changes in (b) average precipitation contributed from  
 392 each region (b) and (c) their average contribution ratios (c) in the dry years between 1998-2019 and  
 393 1980-1997. ‘\*\*\*’ and ‘\*’ represent 0.05 and 0.1 level significance of the difference.

#### 394 4. Discussion

395 The trends in the contribution from the three source regions, the local, the west  
 396 and the east regions, to all seasonal and annual precipitation over the past 40 years are  
 397 listed in Table 1. In general, the decreasing trend maintained by the local IP and the east  
 398 region are closely related to the drought in the Mediterranean basin (Ribeiro et al., 2020;  
 399 Russo et al., 2019), and the increasing proportion of the west can be explained by the

400 increasingly important role of the oceanic moisture in terrestrial precipitation (Gimeno  
 401 et al., 2020; Vicente-Serrano et al., 2018). The simultaneous decrease in the moisture  
 402 contribution from all three regions is responsible for the significant decrease in only the  
 403 summer precipitation series among all seasonal or annual precipitation. In particular,  
 404 the local [moisture](#) recycling ratio in summer is obviously way down, differentiating the  
 405 reduced summer precipitation from the other seasons. It is worth highlighting that this  
 406 significant decrease in recent summer precipitation over the IP in this study is based on  
 407 a short record (1980-2019) from ERA5, while a long-term assessment of precipitation  
 408 (1850-2018) from multiple sources still lacks a statistically significant decreasing trend  
 409 (Peña-Angulo et al., 2020). Nevertheless, the changes in the recent four decades still  
 410 show the significant influence of the local [moisture](#) recycling, especially on the trend  
 411 of summer precipitation and variation of summer wet and dry years.

412

413 **Table 1** Trends of contributions from the IP, the west and the east to annual and seasonal  
 414 precipitation, and the trends of their contribution ratios.

	Contributed precipitation (mm mon <sup>-1</sup> decade <sup>-1</sup> )					Contribution ratio (% decade <sup>-1</sup> )				
	Annual	Spring	Summer	Autumn	Winter	Annual	Spring	Summer	Autumn	Winter
IP	-0.24**	-0.30	-0.59**	-0.03	-0.03	-0.49**	-0.66**	-1.17**	-0.14	-0.08
West	0.53	1.67	-1.28*	1.23	0.52	0.81**	0.80	1.29**	0.38	0.77
East	-0.17	-0.06	-0.28	-0.05	-0.29	-0.32	-0.14	-0.12	-0.24	-0.69

415 \*\*\* and \*\* represent 0.05 and 0.1 level significance of the trend.

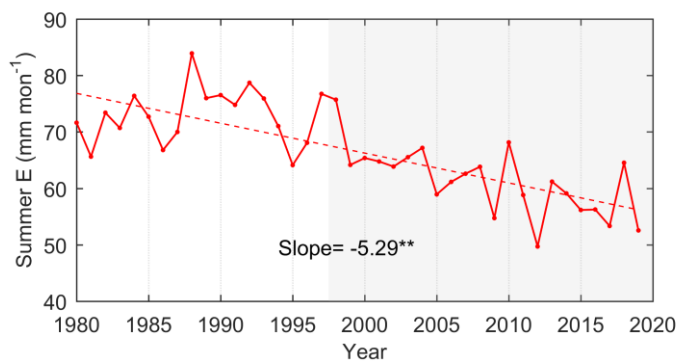
416 The remarkable decrement of summer precipitation can be attributed to the

417 simultaneous and large reduction of contributions from all three source regions.  
418 Moisture transport from the west region contributing to the IP precipitation is mainly  
419 through the tropical–subtropical North Atlantic corridor. In summer, air masses from  
420 the west in this transportation process, as it gets closer to the destination, gradually shift  
421 from a net supply to a net uptake of the IP precipitation (Gimeno et al., 2010). In this  
422 case, ~~the~~ stronger land-sea contrast caused by the warming land surface makes the  
423 advected air mass from the Atlantic experience more drying (~~Cramer et al., 2018;~~  
424 ~~Kröner et al., 2017~~), and resulting in a decrease in the moisture contribution from the  
425 Atlantic Ocean in the west (Cramer et al., 2018; Kröner et al., 2017) to the IP  
426 precipitation. In addition, the extension of Hadley circulation makes the IP more  
427 strongly affected by subsidence, with generating higher static stability (Brogli et al.,  
428 2019). This results in a ~~and~~ lower frequency of extreme heavy precipitation  
429 characterized by the presence of a cutoff low at mid-levels and an easterly moisture  
430 flow from the Mediterranean Sea (Merino et al., 2016). (~~Brogli et al., 2019~~). However,  
431 the ocean warming patterns and thermodynamics can promote precipitation in cold  
432 seasons (Brogli et al., 2019), just as shown by the increasing contributed precipitation  
433 from the west in autumn and winter in Table 1. It suggests the drivers leading to less  
434 summer precipitation do not generally cause a similar change in the precipitation in the  
435 other seasons.

436 In terms of the total contribution from the three subregions, the west region  
437 dominates more of the reduction in the IP precipitation due to its wide coverage with a

438 large number of grids. Nevertheless, in the local IP, which is much smaller than the  
439 west, the high contribution per grid, the difference between the two periods, and the  
440 consistent decline of the precipitation recycling ratio make the role of the local  
441 contribution variation worth emphasizing. As an important indicator to describe the  
442 interaction between the surface and atmospheric processes, the change in the  
443 precipitation recycling ratio takes into account changes in both precipitation and the  
444 contribution of local evaporation (Goessling and Reick, 2011; Zhang, 2020). For the IP,  
445 its significant reduction in local moisture contribution is most likely due to the  
446 weakening of local evaporation (Fig. 9), with a correlation coefficient of 0.64 between  
447 evaporation and the locally contributed precipitation. In summer, soil moisture and the  
448 recycling process driven by evaporation are regarded as an active source of moisture  
449 (Jung et al., 2010; Vicente-Serrano et al., 2014). ~~Due to,~~ leading to the positive  
450 correlation between soil moisture and precipitation ~~in summer,~~ As a result, during those  
451 dry summers, the declining precipitation ~~leads to~~ causes the shortage of soil water  
452 supply, the limitation of soil water evaporation capacity and the consequent reduction  
453 in surface evaporation (García-Valdecasas Ojeda et al., 2020; Ruosteenoja et al., 2018).  
454 ~~Epecially in summer, when the soil moisture and recycling process driven by~~  
455 ~~evaporation are regarded as an active source of moisture (Jung et al., 2010; Vicente~~  
456 ~~Serrano et al., 2014).~~ The IP precipitation can be further reduced due to this weakening  
457 of the local moisture recycling ~~again leads to a decrease in precipitation.~~ This  
458 continuous feedback of the interactions of soil moisture evaporation and precipitation

459 can exacerbate the water resource depletion and summer drought, [especially in dry](#)  
460 [years. Thus, despite the ongoing emphasis on the significance of the ocean as a moisture](#)  
461 [source, consistent changes in the local moisture contribution or proportion with reduced](#)  
462 [precipitation require more attention.](#)



463  
464 **Figure 9** Time series of [the](#) IP summer evaporation from [the](#) ERA5 during 1980-2019 (unit of the  
465 slope: mm mon<sup>-1</sup> decade<sup>-1</sup>). \*\*\* represents 0.05 level significance of the trend.

## 466 5. Conclusions

467 [Decreasing summer precipitation over the IP could lead to an escalation of drought,](#)  
468 [especially with the high temperature and low rainfall characteristics of Mediterranean](#)  
469 [climate.](#) In this study, using the reanalysis data ERA5 and WAM-2layers model, we  
470 investigated how changes in moisture contribution from the sources, [including the IP,](#)  
471 [the west and the east,](#) affect the reduction in summer precipitation between 1980-1997  
472 and 1998-2019. The major findings [attribute the decreasing precipitation to the changes](#)  
473 [in moisture contribution at source and highlight their importance, which](#) are  
474 summarized below.

475 1) The reduction of contribution to IP summer precipitation is mainly concentrated in  
476 the IP and its neighboring grids. The local IP grids show the greatest reduction, and  
477 the surrounding grids show a slight but significant decrease.

478 2) Compared with the ~~period~~-summer of 1980-1997, the IP and the east contributed  
479 1.7 and 1.1 mm mon<sup>-1</sup> less IP precipitation during 1998-2019, accounting for 26%  
480 and 17% of the main source supply reduction, respectively. Meanwhile, the  
481 importance of the vast west region was clearly shown by reducing the IP  
482 precipitation by 3.6 mm mon<sup>-1</sup>, representing 57% of the decrease in precipitation  
483 originating from main sources.~~the decrease in the moisture contribution from the IP,~~  
484 ~~the west and the east during 1998-2019 results in the reductions of 1.7, 3.6, and 1.1~~  
485 ~~mm mon<sup>-1</sup> of the IP precipitation, accounting for 26%, 57%, and 17% of the main~~  
486 ~~source supply reduction, respectively.~~

487 3) The contributions from the local IP and the east keep declining during the 40 years.  
488 In particular, the significant reduction in the local moisture recycling, reflected in  
489 the disappearance of the wet years after 1997 and the reduction of local  
490 contributions in the dry years, suggests a close link with the decrease in summer  
491 precipitation.

492

### 493 **Code and Data availability**

494 Code and data used in this manuscript are available from the corresponding author upon  
495 a reasonable request.

496

497 **Author contributions**

498 MG and QT designed the study; YL performed the analysis and calculation; CZ  
499 contributed to the application of the model in this study; YL prepared the manuscript  
500 draft, and all co-authors reviewed and edited the manuscript.

501

502 **Competing interests**

503 The authors declare no competing interests.

504

505 **Acknowledgements**

506 This study was partly funded by the National Natural Science Foundation of China  
507 (41730645) and the Strategic Priority Research Program of Chinese Academy of  
508 Sciences (XDA20060402). The authors would like to thank the EU and Innovation  
509 Fund Denmark (IFD) for funding within the framework of the FORWARD  
510 collaborative international consortium financed through the ERA-NET co-fund  
511 WaterWorks2015 integral part of the 2016 joint activities developed by the “Water  
512 Challenges for a Changing World” joint programme initiative (Water JPI).

513

514 **References**

- 515 Boé, J., and Terray, L.: Land–sea contrast, soil-atmosphere and cloud-temperature  
516 interactions: interplays and roles in future summer European climate change,  
517 *Clim. Dyn.*, 42, 683-699, <https://doi.org/10.1007/s00382-013-1868-8>, 2014.
- 518 Boé, J., Terray, L., Cassou, C., and Najac, J.: Uncertainties in European summer  
519 precipitation changes: role of large scale circulation, *Clim. Dyn.*, 33, 265-276,  
520 <https://doi.org/10.1007/s00382-008-0474-7>, 2009.
- 521 Bonne, J. L., Masson-Delmotte, V., Cattani, O., Delmotte, M., and Steen-Larsen, H. C.:  
522 The isotopic composition of water vapour and precipitation in Ivittuut, Southern  
523 Greenland, *Atmos. Chem. Phys.*, 14, 4419-2014, <https://doi.org/10.5194/acp-14-4419-2014>, 2014.
- 524  
525 Brogli, R., Sørland, S. L., Kröner, N., and Schär, C.: Causes of future Mediterranean  
526 precipitation decline depend on the season, *Environ. Res. Lett.*, 14, 114017,  
527 <https://doi.org/10.1088/1748-9326/ab4438>, 2019.
- 528 Burde, G. I.: Bulk recycling models with incomplete vertical mixing. Part I: Conceptual  
529 framework and models, *J. Clim.*, 19, 1461-1472,  
530 <https://doi.org/10.1175/jcli3687.1>, 2010.
- 531 Cortesi, N., Trigo, R. M., Gonzalez-Hidalgo, J. C., and Ramos, A. M.: Modeling  
532 monthly precipitation with circulation weather types for a dense network of  
533 stations over Iberia, *Hydrol. Earth Syst. Sci.*, 17, 665-678,  
534 <https://doi.org/10.5194/hess-17-665-2013>, 2013.
- 535 Cramer, W., Guiot, J., Fader, M., Garrabou, J., Gattuso, J.-P., Iglesias, A., . . . Xoplaki,  
536 E.: Climate change and interconnected risks to sustainable development in the  
537 Mediterranean, *Nat. Clim. Chang.*, 8, 972-980, <https://doi.org/10.1038/s41558-018-0299-2>, 2018.
- 538  
539 Damián, I.-C., and Gonzalo, M. M.: A new moisture tagging capability in the Weather  
540 Research and Forecasting model: formulation, validation and application to the  
541 2014 Great Lake-effect snowstorm, *Earth Syst. Dynam.*, 9, 167-185,  
542 <https://doi.org/10.5194/esd-9-167-2018>, 2018.
- 543 García-Valdecasas Ojeda, M., Yeste, P., Gámiz-Fortis, S. R., Castro-Díez, Y., and  
544 Esteban-Parra, M. J.: Future changes in land and atmospheric variables: An  
545 analysis of their couplings in the Iberian Peninsula, *Sci. Total Environ.*, 722,  
546 137902, <https://doi.org/10.1016/j.scitotenv.2020.137902>, 2020.
- 547 Gimeno, L., Nieto, R., and Sorí, R.: The growing importance of oceanic moisture  
548 sources for continental precipitation, *npj Clim. Atmos. Sci.*, 3, 27,  
549 <https://doi.org/10.1038/s41612-020-00133-y>, 2020.
- 550 Gimeno, L., Nieto, R., Trigo, R. M., Vicente-Serrano, S. M., and López-Moreno, J. I.:  
551 Where does the Iberian Peninsula moisture come from? An answer based on a  
552 Lagrangian approach, *J. Hydrometeorol.*, 11, 421-436,  
553 <https://doi.org/10.1175/2009JHM1182.1>, 2010.

554 Goessling, H. F., and Reick, C. H.: What do moisture recycling estimates tell us?  
 555 Exploring the extreme case of non-evaporating continents, *Hydrol. Earth Syst.*  
 556 *Sci.*, 15, 3217-3235, <https://doi.org/10.5194/hess-15-3217-2011>, 2011.

557 Goessling, H. F., and Reick, C. H.: On the "well-mixed" assumption and numerical 2-  
 558 D tracing of atmospheric moisture, *Atmos. Chem. Phys.*, 13, 5567-5585,  
 559 <https://doi.org/10.5194/acp-13-5567-2013>, 2013.

560 Herrera, S., Cardoso, R. M., Soares, P. M., Espírito-Santo, F., and Gutiérrez, J.: Iberia01:  
 561 a new gridded dataset of daily precipitation and temperatures over Iberia, *Earth*  
 562 *Syst. Sci. Data*, 11, 1947-1956, <https://doi.org/10.5194/essd-11-1947-2019>,  
 563 2019.

564 Hersbach, H., Bell, B., Berrisford, P., Hirahara, S., Horányi, A., Muñoz-Sabater, J., . . .  
 565 Thépaut, J.-N.: The ERA5 global reanalysis, *Quarterly Journal of the Royal*  
 566 *Meteorological Society*, 146, 1999-2049, <https://doi.org/10.1002/qj.3803>, 2020.

567 Jung, M., Reichstein, M., Ciais, P., Seneviratne, S. I., Sheffield, J., Goulden, M. L., . . .  
 568 Zhang, K.: Recent decline in the global land evapotranspiration trend due to  
 569 limited moisture supply, *Nature*, 467, 951-954,  
 570 <https://doi.org/10.1038/nature09396>, 2010.

571 Keys, P. W., Gordon, L. J., . . . R.: Variability of moisture recycling using a  
 572 precipitationshed framework, *Hydrol. Earth Syst. Sci.*, 18, 3937-3950,  
 573 <https://doi.org/10.5194/hess-18-3937-2014>, 2014.

574 Keys, P. W., Ent, R., Gordon, L. J., Hoff, H., and Savenije, H.: Analyzing  
 575 precipitationsheds to understand the vulnerability of rainfall dependent regions,  
 576 *Biogeosciences*, 8, 733-746, <https://doi.org/10.5194/bg-9-733-2012>, 2011.

577 Kröner, N., Kotlarski, S., Fischer, E., Lüthi, D., Zubler, E., and Schär, C.: Separating  
 578 climate change signals into thermodynamic, lapse-rate and circulation effects:  
 579 theory and application to the European summer climate, *Clim. Dyn.*, 48, 3425-  
 580 3440, <https://doi.org/10.1007/s00382-016-3276-3>, 2017.

581 Lenderink, G., van Ulden, A., van den Hurk, B., and van Meijgaard, E.: Summertime  
 582 inter-annual temperature variability in an ensemble of regional model  
 583 simulations: analysis of the surface energy budget, *Clim. Change*, 81, 233-247,  
 584 <https://doi.org/10.1007/s10584-006-9229-9>, 2007.

585 Lopez-Bustins, J. A., and Lemus-Canovas, M.: The influence of the Western  
 586 Mediterranean Oscillation upon the spatio-temporal variability of precipitation  
 587 over Catalonia (northeastern of the Iberian Peninsula), *Atmos. Res.*, 236,  
 588 104819, <https://doi.org/10.1016/j.atmosres.2019.104819>, 2020.

589 [Merino, A., Fernández-Vaquero, M., López, L., Fernández-González, S., Hermida, L.,](https://doi.org/10.1002/joc.4601)  
 590 [Sánchez, J. L., . . . Gascón, E.: Large-scale patterns of daily precipitation](https://doi.org/10.1002/joc.4601)  
 591 [extremes on the Iberian Peninsula, \*International Journal of Climatology\*, 36,](https://doi.org/10.1002/joc.4601)  
 592 [3873-3891, \[https://doi.org/https://doi.org/10.1002/joc.4601\]\(https://doi.org/10.1002/joc.4601\), 2016.](https://doi.org/10.1002/joc.4601)

593 Numaguti, A.: Origin and recycling processes of precipitating water over the Eurasian  
 594 continent: Experiments using an atmospheric general circulation model, *J.*

设置了格式: 字体: (中文) + 中文正文 (等线)

595 Geophys. Res.-Atmos., 104, 1957-1972,  
596 <https://doi.org/10.1029/1998JD200026>, 1999.

597 Páscoa, P., Russo, A., Gouveia, C. M., Soares, P. M. M., Cardoso, R. M., Careto, J. A.  
598 M., and Ribeiro, A. F. S.: A high-resolution view of the recent drought trends  
599 over the Iberian Peninsula, *Weather Clim. Extremes*, 32, 100320,  
600 <https://doi.org/10.1016/j.wace.2021.100320>, 2021.

601 Peña-Angulo, D., Vicente-Serrano, S. M., Domínguez-Castro, F., Murphy, C., Reig, F.,  
602 Trambly, Y., . . . El Kenawy, A.: Long-term precipitation in Southwestern  
603 Europe reveals no clear trend attributable to anthropogenic forcing, *Environ.*  
604 *Res. Lett.*, 15, 094070, <https://doi.org/10.1088/1748-9326/ab9c4f>, 2020.

605 Rajczak, J., and Schär, C.: Projections of future precipitation extremes over Europe: A  
606 multimodel assessment of climate simulations, *J. Geophys. Res.-Atmos.*, 122,  
607 10,773-710,800, <https://doi.org/10.1002/2017JD027176>, 2017.

608 Ribeiro, A. F. S., Russo, A., Gouveia, C. M., and Pires, C. A. L.: Drought-related hot  
609 summers: A joint probability analysis in the Iberian Peninsula, *Weather Clim.*  
610 *Extremes*, 30, 100279, <https://doi.org/10.1016/j.wace.2020.100279>, 2020.

611 Ruosteenoja, K., Markkanen, T., Venäläinen, A., Räisänen, P., and Peltola, H.: Seasonal  
612 soil moisture and drought occurrence in Europe in CMIP5 projections for the  
613 21st century, *Clim. Dyn.*, 50, 1177-1192, [https://doi.org/10.1007/s00382-017-](https://doi.org/10.1007/s00382-017-3671-4)  
614 [3671-4](https://doi.org/10.1007/s00382-017-3671-4), 2018.

615 Russo, A., Gouveia, C. M., Dutra, E., Soares, P. M. M., and Trigo, R. M.: The synergy  
616 between drought and extremely hot summers in the Mediterranean, *Environ.*  
617 *Res. Lett.*, 14, 014011, <https://doi.org/10.1088/1748-9326/aaf09e>, 2019.

618 Serrano, A., García, J. A., Mateos, V. L., Cancillo, M. L., and Garrido, J.: Monthly  
619 modes of variation of precipitation over the Iberian Peninsula, *J. Clim.*, 12,  
620 2894-2919, 1999.

621 Stohl, A., and James, P.: A Lagrangian analysis of the atmospheric branch of the global  
622 water cycle. Part I: Method description, validation, and demonstration for the  
623 August 2002 flooding in Central Europe, *J. Hydrometeorol.*, 5, 656, 2004.

624 Stohl, A., and James, P.: A Lagrangian analysis of the atmospheric branch of the global  
625 water cycle. Part II: Moisture transports between earth's ocean basins and river  
626 catchments, *J. Hydrometeorol.*, 6, 961-984, <https://doi.org/10.1175/JHM470.1>,  
627 2005.

628 Tang, Q., Leng, G., and Groisman, P. Y.: European hot summers associated with a  
629 reduction of cloudiness, *J. Clim.*, 25, 3637-3644, [https://doi.org/10.1175/JCLI-](https://doi.org/10.1175/JCLI-D-12-00040.1)  
630 [D-12-00040.1](https://doi.org/10.1175/JCLI-D-12-00040.1), 2012.

631 Teuling, A. J., Van Loon, A. F., Seneviratne, S. I., Lehner, I., Aubinet, M., Heinesch,  
632 B., . . . Spang, U.: Evapotranspiration amplifies European summer drought,  
633 *Geophys. Res. Lett.*, 40, 2071-2075, <https://doi.org/10.1002/grl.50495>, 2013.

634 Ulbrich, U., Christoph, M., Pinto, J. G., and Corte-Real, J.: Dependence of winter  
635 precipitation over Portugal on NAO and baroclinic wave activity, *International*

636 Journal of Climatology, 19, 379-390, [https://doi.org/10.1002/\(SICI\)1097-](https://doi.org/10.1002/(SICI)1097-)  
637 [0088\(19990330\)19:4<379::AID-JOC357>3.0.CO;2-8](https://doi.org/10.1002/(SICI)1097-0088(19990330)19:4<379::AID-JOC357>3.0.CO;2-8), 2015.

638 van der Ent, R. J., and Savenije, H. H. G.: Length and time scales of atmospheric  
639 moisture recycling, *Atmos. Chem. Phys.*, 11, 1853-1863,  
640 <https://doi.org/10.5194/acp-11-1853-2011>, 2011.

641 van der Ent, R. J., Savenije, H. H. G., Schaefli, B., and Steele-Dunne, S. C.: Origin and  
642 fate of atmospheric moisture over continents, *Water Resour. Res.*, 46,  
643 <https://doi.org/10.1029/2010WR009127>, 2010.

644 van der Ent, R. J., Tuinenburg, O. A., Knoche, H. R., Kunstmann, H., and Savenije, H.  
645 H. G.: Should we use a simple or complex model for moisture recycling and  
646 atmospheric moisture tracking?, *Hydrol. Earth Syst. Sci.*, 17, 4869-4884,  
647 <https://doi.org/10.5194/hess-17-4869-2013>, 2013.

648 van der Ent, R. J., Wang-Erlandsson, L., Keys, P., and Savenije, H.: Contrasting roles  
649 of interception and transpiration in the hydrological cycle - Part 2: Moisture  
650 recycling, *Earth Syst. Dynam.*, 5, <https://doi.org/10.5194/esdd-5-281-2014>,  
651 2014.

652 [Vázquez, M., Nieto, R., Liberato, M. L. R., and Gimeno, L.: Atmospheric moisture](https://doi.org/https://doi.org/10.1016/j.wace.2020.100289)  
653 [sources associated with extreme precipitation during the peak precipitation](https://doi.org/https://doi.org/10.1016/j.wace.2020.100289)  
654 [month, \*Weather and Climate Extremes\*, 30, 100289,](https://doi.org/https://doi.org/10.1016/j.wace.2020.100289)  
655 <https://doi.org/https://doi.org/10.1016/j.wace.2020.100289>, 2020.

656 Vicente-Serrano, S. M., Azorin-Molina, C., Sanchez-Lorenzo, A., Morán-Tejeda, E.,  
657 Lorenzo-Lacruz, J., Revuelto, J., . . . Espejo, F.: Temporal evolution of surface  
658 humidity in Spain: recent trends and possible physical mechanisms, *Clim. Dyn.*,  
659 42, 2655-2674, <https://doi.org/10.1007/s00382-013-1885-7>, 2014.

660 Vicente-Serrano, S. M., Nieto, R., Gimeno, L., Azorin-Molina, C., Drumond, A., El  
661 Kenawy, A., . . . Peña-Gallardo, M.: Recent changes of relative humidity:  
662 regional connections with land and ocean processes, *Earth Syst. Dynam.*, 9,  
663 915-937, <https://doi.org/10.5194/esd-9-915-2018>, 2018.

664 [Zhang, C.: Moisture source assessment and the varying characteristics for the Tibetan](https://doi.org/10.1088/1748-9326/abac78)  
665 [Plateau precipitation using TRMM, \*Environ. Res. Lett.\*, 15, 104003,](https://doi.org/10.1088/1748-9326/abac78)  
666 <https://doi.org/10.1088/1748-9326/abac78>, 2020.

667 [Zhang, C., Tang, Q., and Chen, D.: Recent changes in the moisture source of](https://doi.org/10.1175/JCLI-D-15-0842.1)  
668 [precipitation over the Tibetan Plateau, \*J. Clim.\*, 30, 1807-1819,](https://doi.org/10.1175/JCLI-D-15-0842.1)  
669 <https://doi.org/10.1175/JCLI-D-15-0842.1>, 2017.

670 [Zhang, Y., Huang, W., Zhang, M., Tian, Y., Wang, G., and Zhong, D.: Atmospheric](https://doi.org/10.1029/2020JD032796)  
671 [Basins: Identification of Quasi-Independent Spatial Patterns in the Global](https://doi.org/10.1029/2020JD032796)  
672 [Atmospheric Hydrological Cycle Via a Complex Network Approach, \*J.\*](https://doi.org/10.1029/2020JD032796)  
673 [\*Geophys. Res.-Atmos.\*, 125, e2020JD032796,](https://doi.org/10.1029/2020JD032796)  
674 [https://doi.org/https://doi.org/10.1029/2020JD032796](https://doi.org/10.1029/2020JD032796), 2020.

675 Zhu, Y., and Newell, R. E.: A proposed algorithm for moisture fluxes from atmospheric  
676 rivers, *Mon. Weather Rev.*, 126, 725-735, <https://doi.org/10.1175/1520->

677 [0493\(1998\)126<0725:Apafmf>2.0.Co;2](#), 1998.  
678